Chapter 2
High-Entropy Film Alloys: Electrophysical and Magnetoresistive Properties

Yu. Bereznyak, L. Odnodvorets, D. Poduremne, I. Protsenko, and Yu. Shabelnyk

2.1 Introduction

In the last decade, research was carried out on the crystal structure and mechanical properties of a new class of materials—high-entropy alloys (HEA)—whose improved properties were first noticed by the authors [12]. Since these alloys are formed from 5 to 13 elements with face centric cubic (fcc), base centric cubic (bcc), or hexagonal (hcp) lattice, they have high entropy of mixing (ΔS_{mix}), and have more stable phase as a bcc or fcc solid solution (s.s.) compared to intermetallic compounds and other complex structures (see, e.g., [4]).

In a bulk AlCrFeCoNiCu high-entropy alloy can simultaneously stabilize the fcc and bcc s.s [2, 4, 5] or bcc s.s. α-Fe(Cr) and intermetallic AlNi [11] depending on the concentration of some component (e.g., atoms Ni).

The authors [4] concluded that stabilizing the fcc or bcc completely determined by the average concentration of valence electrons per atom located in the valence band of the alloy. At the concentration less than 7.2 el/at bcc phase formed, at 7.2–8.2 el/at two-phase composition fcc + bcc stabilized and at concentrations greater than 8.2 el/at—fcc phase s.s. HEA.

The peculiarity of our experiments consists in the fact that formation of s.s. made by layered or simultaneous deposition of some individual components of thickness up to 8 nm (total thickness up to 60 nm), which, thanks to condensation-stimulated diffusion and low thickness, causes mixing of atoms and forming of s.s.

Yu. Bereznyak · L. Odnodvorets · D. Poduremne · I. Protsenko (✉) · Yu. Shabelnyk
Department of Electronics, General and Applied Physics, Sumy State University, Sumy, Ukraine
e-mail: i.protsenko@aph.sumdu.edu.ua

The aim of our work was to study phase state, electrophysical and magnetoresistivity properties of high-entropy film alloys, which was established in our previous work [10].

2.2 Methodology and Techniques Experiment

The film samples are condensed by controlling the thickness of the layers by quartz crystal method. For the diffraction and electron-microscopic studies, C-substrate (S) was used, and for the resistance and magnetoresistance measured, sitall-substrates were used.

Strain coefficient was measured by the method [9] using polystyrene substrates. The concentration of component was calculated and refined by energy dispersive X-ray (EDX) analysis. The calculation was performed on the ratio

$$C_i = \frac{D_i d_i \mu_i^{-1}}{\sum\limits_{i=1}^{n} D_i d_i \mu_i^{-1}},$$

where D is density, μ is molar mass, d is thickness of individual layers at the layered deposition or effective thickness at the simultaneous deposition.

It is known (see, e.g., [6, 13]) that the formation of HEA occurs under the following conditions: the value of ΔS_{mix} should be greater than $\Delta S_{mix} = 1.61$ $R = 13.38$ J/(mole·K) (for five-component alloys) or $\Delta S_{mix} = 1.75$ $R = 14.54$ J/(mol·K) (for six-component alloys) and parameters of atomic size differences

$$\delta = \sqrt{\sum_{i=1}^{n} c_i \left(1 - \frac{r_i}{\overrightarrow{r}}\right)^2},$$

where r_i is the atomic radius of i-component; $\overrightarrow{r} = \sqrt{\sum\limits_{i=1}^{n} c_i r_i}$, the average atomic radius, should be less than 6.6% (in our case, these conditions are fulfilled).

Calculation of mixing entropy (ΔS_{mix}) as a criterion of HEA was performed on ratio [13] (see also [4])

$$\Delta S_{mix} = -R \sum_{i=1}^{n} c_i \ln c_i,$$

where i and c_i are the number and atomic concentrations of i-components.

Table 2.1 shows general characteristics of the samples. Note that the No 1′ and No 2′ samples with seven components are different from the six-component No 1 and No 2 samples only by the additional layer of Ti. Also note that the elemental

Table 2.1 General characteristics of HEA films

№	Sample (thickness, nm)	c_i, at. %	ΔS_{mix}, J/(mol·K)	TCR·10^3, K^{-1} at $T = 300$ K
1	Cr(7.5)/Al(4.5)/Co(7.3)/Cu(4.8)/Ni (7.0)/Fe(7.0)/S	19/8/21/12/19/19/S	14.58	1.80
1′	Ti(2.2)/Cr(7.5)/Al(4.5)/Co(7.3)/Cu (4.8)/Ni(7.0)/Fe(7.0)/S	4/18/9/20/12/19/18/S	15.33	1.75
2	Al(4.0)/Cu(3.2)/Co(4.5)/Cr(5.2)/Fe (4.7)/Ni(4.0)/S	11/13/19/20/19/17/S	14.76	2.00
2′	Ti(2.5)/Al(4.0)/Cu(3.2)/Co(4.5)/Cr (5.2)/Fe(4.7)/Ni(4.0)/S	6/11/12/18/18/19/16/S	15.54	1.75
3	Cr(10)/Fe(9)/Ni(10)/S	33/30/37/S	9.12	1.20
4	Cu(32)/Co(9)/Cr(10)/Ni$_{0.8}$Fe$_{0.2}$(19)/Al (12)/S	32/15/16/19/5/14/S	14.02	1.80
5	Cu(10)/Co(9)/Cr(10)/Ni$_{0.8}$Fe$_{0.2}$(19)/Al (12)/S	18/17/17/24/8/15/S	14.38	1.22

composition of No. 1 and No. 2 samples corresponds to samples studied by the authors of [4, 11]. We will indicate that the permalloy (Py) Ni$_{0.8}$Fe$_{0.2}$ as a separate layer has been selected in order to determine whether Py is stored as a separate layer in the HEA, or dissociation of the NiFe complexes in the film occurs. As we have established, there is a dissociation of these complexes (Sect. 2.3.1). According to [1], the magnitude of the enthalpy of mixing ΔH_{mix} can make a prognosis of the phase state of the HEA: solid solution, ordered phase, or chemical compound.

The thermal coefficient of resistance (TCR) was calculated based on the temperature dependence on the resistivity (ρ) (the second temperature cycle at the cooling) and the ratio

$$\beta = \frac{\rho(T) - \rho(300)}{\rho(300)(T - 300)}.$$

Integral value of strain coefficient determined based on depending $\Delta R/R(0)$ versus on the value of longitudinal strain ε_l on the ratio

$$\gamma_l = \frac{R(\varepsilon_l) - R(0)}{R(0)\varepsilon_l}.$$

The value of magnetoresistance (MR) calculated on the basis of field dependence $R(B)$ on the ratio

$$MR = \frac{R(B) - R(0)}{R(0)}.$$

To measure $\rho(T)$, $R(\varepsilon_l)$, and $R(B)$ and calculate β, γ_l and MR used appropriate computerized complex.

2.3   Results and Discussion

2.3.1   Crystalline Structure

Electron microscopic study indicates that in the initial state (after condensation) the crystal structure are high-disperse (the average crystallite size L $\leq$ 10 nm). Beside with the high-disperse fraction is formed a structure with L $\cong$ 50 nm after annealing to 850 K (Fig. 2.1). The character of electron diffraction indicates that at the stage of condensation in HEA film, two fcc and one bcc phases (so-called B2 phase) were formed. A similar phase composition was observed by [4]. The fcc1 and fcc2 phases formation associated with the unfinished process of s.s. HEA formation. Although with annealing of the samples to 850 K homogenization alloy appears and s.s. HEA forms with fcc lattice based on the fcc1 and fcc2 (the lattice parameter $a = 0.3604$ nm) (Fig. 2.1, Table 2.2). Most likely, one of the fcc phases initially formed as s.s. HEA, the other was a metastable phase based on Al and Ni [11], which decomposited during annealing. According to conclusions [11] bcc phase can be magnetic s.s. α-Fe (Cr). The gray background between the diffraction lines (111) and (200) indicates its specific nonuniformity and vacancy defect.
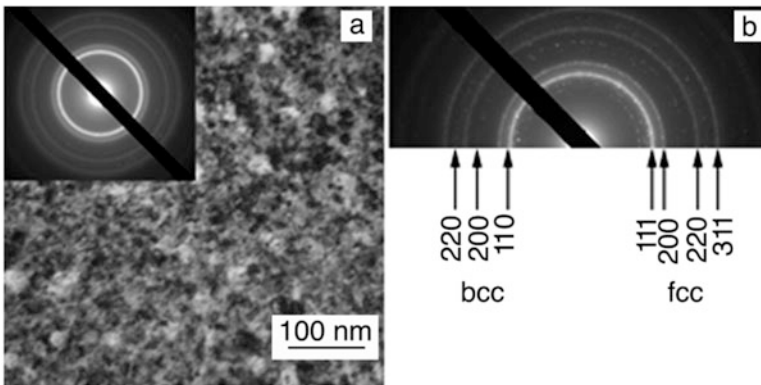
Fig. 2.1 Microstructure and diffraction pattern from system Cr(7.5)/Al(4.5)/Co(7.3)/Cu(4.8)/Ni (7.0)/Fe(7.0)/S. Annealing temperature, K: 600 (**a**) and 850 (**b**)

Table 2.2 Decryption of diffraction pattern from HEA

№	d_{hkl}, nm	hkl	a, nm	Phase
1	0.2175	111	0.3616	s.s.
2	0.2088	200	0.3600	s.s.
3	0.1420	200	0.2840	bcc
4	0.1272	220	0.3597	s.s.
5	0.1010	220	0.2850	bcc
6	0.10870	311	0.3605	s.s.
			a(s.s.) = 0.3604 nm	

Annealing of samples contributes to the healing of defects and some ordering s.s. and leads to the formation of a small number of Al_2O_3 oxides, ($d_{hkl} = 0.237$ nm) and Cr_2O_3 ($d_{hkl} = 0.261$ and 0.247 nm), whose reflexes are of a point character and of low intensity (not shown in Table 2.2) due to the low effective thickness layers of Cr and Al. In addition, we note that two very weak lines (200) and (220) are recorded from the bcc phase (phase B2), which was observed by the authors [4], and the most intense line (110) is not fixed. Note that the average value of the parameter fcc lattice s.s. is in very good agreement with the corresponding parameter for s.s. Cu(Ni) $a = 0.352$–0.366 nm [3]. Also, we note that the addition of a thin layer of Ti (specimens 1'and 2') or Py (see 4 and 5) does not affect their phase composition.

It is known (see, e.g., [6, 13]) that the formation of HEA is due to the performance of the following conditions: the value of ΔS_{mix} six-component alloy should be more $\Delta S_{mix} = 1.75\, R = 1454$ J/(mol·K) for equiatomic alloy and parameters of difference in atomic size. The fact that in our case annealed HEA actually has only one fcc phase is explained by the corresponding value of ΔS_{mix} and δ. It should also be noted that the described phase composition does not depend on the method of film material formation—simultaneous or layered condensation—which is explained by the active mixing of the components in the process of deposition.

2.3.2 Electrophysical Properties

Figure 2.2 shows the typical dependence of resistivity and TCR (insert) for HEA. The typical features of the samples are: the relatively large value of the TCR (order of magnitude 10^{-3} K^{-1}) and the defect concentration of the crystalline structure of the «vacancy-intersite atom» type, which is indicated by the reduction of the specific resistance during ignition in the I cycle of «heating ↔ cooling».

During the study of strain coefficient (SC) of HEA, we, probably, first observed the strain effect feature. At the strain in the range $\Delta\varepsilon_l = (0–1)$ % at the $\varepsilon'_{ltr} \cong 0.5\%$ transition from elastic to plastic strain occurs (we call it plastic strain type I). At the I strain cycle on the range $\Delta\varepsilon_l = (0 - 1)\%$, the value strain coefficient $\gamma_{l,I} \cong 12.0$, and range $\Delta\varepsilon_{l1} \cong (0 - 0.5)\%$, $\gamma_{l,II,III} \cong 25$. In II and III cycles of strain were observed linear dependence of $\Delta R/R(0)$ versus ε_l, value of strain coefficient $\gamma_l \cong 12.5$. At this stage, sold, most likely after the relaxation effect quasiplastic strain of I type. With further strain to $\varepsilon_l = 2\%$ is the transition to plastic strain of II type at $\varepsilon''_{ltr} \cong 1\%$. This transition is accompanied by an increase of value strain coefficient to $\gamma_{l,II,III} \cong 12.5$ to $\gamma_{l,IV} \cong 90$, which is a significant value for metal films. At the V and VI strain cycles, there is also a kind of strain to quasiplastic because there was a relaxation of plastic strain of the II type. The described two-stage feature of the strain effect was not observed in the case of single-layer or multilayer films (see, e.g., reviews [7, 8]) with their plastic deformation.
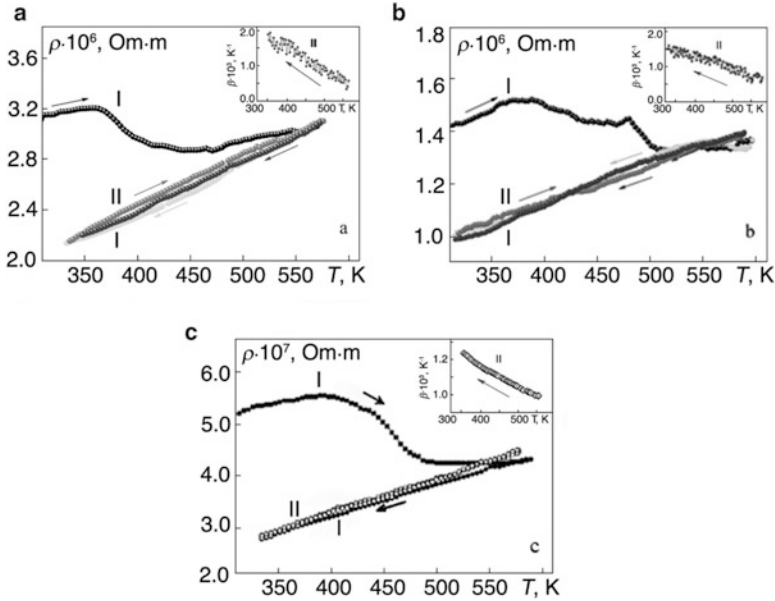
Fig. 2.2 Dependence of resistivity and TCR (insert) versus temperature for samples No. 2 (**a**), No. 2′(**b**), and No. 5 (**c**). I, II—numbers of annealing cycles

2.3.3 Magnetoresistivity Properties

Research of MR was performed in geometry CIP (current j in the film plane) at the three mutual orientation of the magnetic field: longitudinal $(\vec{B} \parallel \vec{j})$, transverse $(\vec{B} + \vec{j})$, and perpendicular $(\vec{B} \perp j)$ at an operating current from 0.5 to 1 mA. Typical dependences of MR on the induction B is shown in Figs. 2.3 and 2.4.

Since bcc HEA is typical ferromagnetic [11], without elements of granular state, it is anisotropic magnetoresistant (AMR), which is clearly shown in Fig. 2.3a and Fig. 2.4 (curve 1) on one side and Fig. 2.3b, c and Fig. 2.4 (curves 2 and 3) on the other side. The effect of annealing to 800 K leads to some increase in the amplitude of the MR with longitudinal and transverse geometries of measurement, while in the case of perpendicular geometry, the amplitude MR practically does not change (Fig. 2.3), although the coercivity decreases significantly. The relatively small amplitude is due to the small thickness (up to 60 nm) and the volume of samples. A very noticeable difference in the shape of the magnetoresistive dependence and the value of the coercive force on Fig. 2.3c and Fig. 2.4 (curve 3) can be explained by the stabilization of planar anisotropy in film alloys.
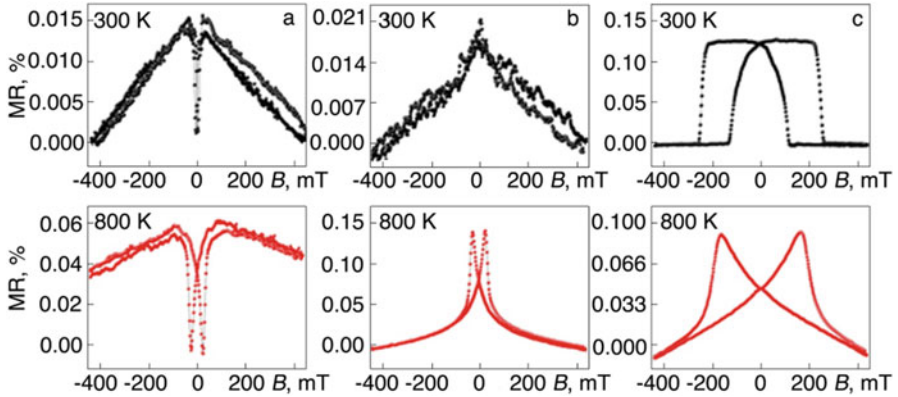
Fig. 2.3 Dependence of MR versus induction B for the sample Al(4.0)/Cu(3.2)/Co(4.5)/Cr(5.2)/ Fe (4.7)/Ni(4.0)/S with three mutual orientations of induction and electric current: longitudinal (**a**), transverse (**b**), and perpendicular (**c**)
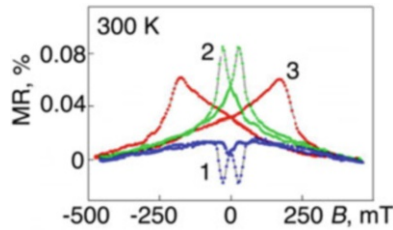
Fig. 2.4 Dependence of MR versus induction B for the sample Cu(10)/Co(9)/Cr(10)/ $Ni_{0.8}Fe_{0.2}$(19)/Al(12)/S with three mutual orientations of induction and electric current: longitudinal (*1*), transverse (*2*), and perpendicular (*3*)

2.4   Conclusions

The crystalline structure, electrophysical (resistivity, TCR, and SC) and magnetic resistive (AMR) properties of HEA films based on Cr, Fe, Al, Cu, Ni, and Co are investigated. It has been established that the films consisted of three phases: fcc1 (s.s. HEA), fcc2 (possibly metastable AlNi) and bcc (possibly s.s. α-Fe(Cr)) after condensation. In the process of annealing fcc2 the phase breaks down, and s.s. α-Fe(Cr) actually disappears, since even weak lines are not fixed on it diffraction pattern.

In the study of electrophysical properties (the strain effect), for the first time, there was a two-stage plastic deformation, each of which corresponds to a very large value of the strain coefficient (up to 90 units); the obscure cause of high sensitivity resistance of s.s. HEA to strain.

The results of the investigation of the magnetoresistive properties unambiguously indicate that the anisotropic MR with a relatively small amplitude up to 0.13% is implemented, which is due to the small thickness of the films.

References

1. Cheng K-H, Weng C-H, Lai C-H, Lin S-J (2009) Study on adhesion and wear resistance of multi-element (AlCrTaTiZr)N coatings. Thin Solid Films 517(17):4989–4993
2. Del Grosso MF, Bozzolo G, Mosca HO (2012) Modeling of high entropy alloys of refractory elements. Physica B 407(16):3285–3287
3. Kalinichenko SM, Tkach OP, Hrychanovska TM, Odnodvorets LV (2015) Thermoresistive properties of the thin film solid solutions based on Cu and Ni. J Nano- Electron Phys 7(4), 04048-1-04048-5
4. Karpets MV, Makarenko OS, Myslyvchenko OM, Krapivka MO, Gorban VF, Samelyuk AV (2014) Properties of multicomponent high-entropy alloy alcrfeconi alloyed copper. Probl Frict Wear 2(63):103–111
5. Li BS, Wang YP, Ren MX, Yang C, Fu HZ (2008) Effects of Mn, Ti and V on the microstructure and properties of AlCrFeCoNiCu high entropy alloy. Mat Sci Eng A 498 (1–2):482–486
6. Pazukha IM, Makukha ZM, Shabelnyk YM, Protsenko IY (2012) Tensoresistive properties of thin film systems based on Ag and Co. J Nano- Electron Phys 4(3), 03020-1-03020-4
7. Protsenko I, Odnodvorets L, Chornous A (1998) Electroconductivity and tensosensibility of multilayer films. Metallofiz Nov Tekhnol 20(1):36
8. Protsenko SI, Odnodvorets LV, Protsenko IY (2014) Nanocomposites, nanophotonics, nanobiotechnology and application. Springer Proc Phys 156:345–374
9. Tyschenko KV, Protsenko IY (2012) Nonlinear effects in piezoresistive features of Fe and Ni based film alloys. Metalofiz Nov Teknol 34(7):907–917
10. Vorobiov SI, Kondrakhova DM, Nepijko SA, Poduremne DV, Shumakova NI, Protsenko IY (2016) Crystalline structure, electrophysical and magnetoresistive properties of high entropy film alloys. J Nano- Electron Phys 8(3), 03026-1-03026-5
11. Wang YP, Li BS, Fu HZ (2009) Solid solution or intermetallics in a high-entropy alloy. Adv Eng Mater 11(8):641–644
12. Yeh JW, Chen SK, Lin SJ, Gan JY, Chin TS, Shun TT, Tsau CH, Chang SY (2004) Nanostructured high-entropy alloys with multiple principal elements: novel alloy design concepts and outcomes. Adv End Mater 6(5):299–303
13. Zhang Y, Zhou Y (2007) Solid solution formation criteria for high entropy alloys. Mater Sci Forum 561–565:1337–1339